

Reflection–absorption FT-IR spectroscopy of pentadecanoic acid at the air/water interface

B.F. Sinnamon^a, R.A. Dluhy^b, G.T. Barnes^{a,*}

^a Department of Chemistry, The University of Queensland, Brisbane, Queensland 4072, Australia

^b Department of Chemistry, University of Georgia, Athens, GA 30602-2556, USA

Received 27 May 1998; accepted 15 September 1998

Abstract

Reflection–absorption Fourier transform infrared (RA FT-IR) spectra of spread monolayers of pentadecanoic acid have been obtained for a range of surface pressures at 292 and 297 K. Unpolarised and *s*- and *p*-polarised radiation at 30° angle of incidence have been used. Results in the C–H stretching region reveal disorder in the arrangement of the acyl chains with numerous *gauche* bonds when the monolayer is in the liquid expanded (LE) phase and highly ordered chains with mostly *trans* bonds in the condensed phases (LC and S). The transition from one form to the other occurs at nearly constant surface pressure in the LE↔LC coexistence region. © 1999 Elsevier Science B.V. All rights reserved.

Keywords: Reflection–absorption FTIR spectroscopy; Monolayers, FTIR spectra; Pentadecanoic acid monolayers; Monolayer structure by FTIR

1. Introduction

Reflection–absorption Fourier transform infrared (RA FT-IR) spectroscopy at the air/water (A/W) interface is now regarded as a sensitive spectroscopic technique that directly measures the molecular-level structure of monolayers in situ at this interface. The technique utilises the reflectance properties of water in the mid-IR region of the electromagnetic spectrum. Theoretical calculations to determine the optimum experimental parameters (e.g. angle of incidence, polarisation)

were developed by Dluhy [1] in 1986 and associated experiments [1–5] have shown that it is possible to acquire spectra with a high signal-to-noise ratio despite the weakness of the RA signals. Reviews by Dluhy [6], Mendelsohn [7] and their collaborators have discussed the development of the theory and described some of the applications of RA FT-IR spectroscopy to the study of monolayers at the air/water interface.

Amphiphiles that have been examined in this way include the fatty acids [8], their esters [9], long-chain alcohols [9], and phospholipids [2–4,10,11]. All of these materials possess a long alkyl chain and it is the RA bands arising from these chains that provide the clearest spectra and

* Corresponding author. Tel.: +61-7-33651511; fax: +61-7-33654299; e-mail: barnes@chemistry.uq.edu.au.

thus the most reliable information about molecular conformation in the monolayer. Bands arising from the polar group of the amphiphile, such as the C=O group, mostly occur in the same spectral region as the absorption bands of water vapour and are difficult to distinguish.

In the 3100–2800 cm^{-1} region of the spectrum, clear RA bands arising from the antisymmetric and symmetric C–H stretching vibrations of the methylene groups of the alkyl chains ($\nu_a(\text{CH}_2)$ and $\nu_s(\text{CH}_2)$, respectively) can be observed with both polarised and unpolarised radiation. The peak positions and peak widths of these bands are sensitive to the relative numbers of *trans* and *gauche* conformers, while the peak heights and peak areas indicate the packing density of the chains. The band for the methyl antisymmetric stretching vibration ($\nu_a(\text{CH}_3)$) is usually visible, but is much weaker than the bands for $\nu_a(\text{CH}_2)$ and $\nu_s(\text{CH}_2)$ as there are fewer such groups in the monolayer. The band for $\nu_s(\text{CH}_3)$ is not usually observed due to overlapping vibrational modes.

In this report RA FT-IR spectroscopy has been used to investigate the conformation of the acyl chains in monomolecular films of pentadecanoic acid (PA) at the A/W interface as a function of the monolayer surface pressure. Qualitative information for the average molecular orientation of the hydrocarbon chain relative to the substrate normal is also obtained.

2. Experimental section

2.1. Materials

Pentadecanoic acid (PA) (Nu-Check Prep.) had a stated purity of >99.0% and was used without further purification. For spreading, it was dissolved in *n*-hexane (Baker Analysed, HPLC grade) at a concentration of 1–3 mg ml^{-1} .

Water for the subphase was obtained from a Barnstead purification system and had a resistivity of $18.3 \pm 0.2 \text{ M}\Omega \text{ cm}$ and pH of 5.8 ± 0.2 at room temperature. The pH of the subphase was adjusted to 2.0 ± 0.2 by addition of HCl (Baker Analysed).

2.2. Equipment

2.2.1. The surface film balance

An automated Langmuir film balance (Joyce-Loebl) interfaced to an IBM-PC compatible computer was used to measure surface pressure—molecular area (Π — $\hat{\text{A}}$) isotherms and also to contain the monolayers for RA FT-IR measurements. This film balance consists of a PTFE trough and uses a constant-perimeter PTFE-coated belt held by six PTFE rollers to confine and compress the monolayer. Surface pressure was measured with a precision of $\pm 0.1 \text{ mN m}^{-1}$ by a paper Wilhelmy plate (Whatman) suspended from a microbalance (Cahn). The temperature was controlled to $\pm 1 \text{ K}$ by pumping thermostatted water through the aluminium base-plate of the trough. During the accumulation of spectra, the surface pressure was maintained automatically to $\pm 1.5 \text{ mN m}^{-1}$.

The instability of PA monolayers above 30 mN m^{-1} meant that the movement of the belt to compensate for the tendency for surface pressure to decrease would allow time for only one spectrum to be accumulated before the belt touched the mirror-mounting accessories.

2.2.2. The RA FT-IR spectrometer

Briefly, the reflection–absorption (RA) infrared experiment employs an infrared beam incident at an angle (θ) to the normal of a monolayer at the A/W interface. The IR beam may be unpolarised or plane-polarised into *s*- (perpendicular to the plane of incidence) or *p*- (parallel to the plane of incidence) components. The Langmuir trough described above was used to form, manipulate and contain the monolayer. It was too large to fit into the sample compartment of the spectrometer so the IR beam was taken from an external port, reflected toward the monolayer at the selected angle (30° with respect to the surface normal), and focussed at the A/W interface. The water surface acts as a reflective element to specularly reflect the IR beam which was then focussed on the detector.

The FT-IR spectrometer (Bio-Rad FTS-60A) and Langmuir trough were mounted on a Newport table top equipped with pneumatic isolation

mounts to stabilise the balance and minimise any disturbance to the monolayer. The internal components of the FT-IR spectrometer were continually purged with dry air. The Langmuir trough, optical path and IR detector were enclosed in a Plexiglass chamber to exclude air-borne contaminants and perturbing air currents.

The reflected radiation was detected by an external narrow-band, liquid-N₂-cooled, mercury-cadmium-telluride (MCT) detector (Model No. HCT-100, Infrared Associates Inc.). The size of the detector chip was as small as possible ($0.25 \times 0.25 \text{ mm}^2$) to minimise detector noise. Polarisation of the IR beam was achieved with a 25 mm aluminium wire-grid polariser on KRS-5 (Model IGP225, Molecron Detector) positioned in a remote controlled (Motor Mike Control Model 18002, ORIEL) rotatable aperture adjacent to the external port of the spectrometer.

To generate a 30° angle of incidence the IR beam from the spectrometer port was directed at the center of a 60° off-axis gold coated parabolic mirror (Janos Technology) which focused the beam to a spot size of approximately 5 mm diameter on the water surface. The optical interface was planned to ensure that the size of the focal point at the A/W interface was consistent throughout a series of experiments. The reflected beam was collected with another 60° off-axis parabolic mirror and focused on the collection mirror of the MCT detector.

2.2.3. Treatment of RA FT-IR data

For all spectra 1024 interferograms were coadded at 4 cm^{-1} optical resolution [1,6]. Each single beam reflectance spectrum required approximately 8 min. The spectra were not smoothed. The coadded interferograms were apodized with a Triangular function and Fourier transformed with one level of zero filling to give data encoded at approximately 2 cm^{-1} . The RA FT-IR spectrum was generated by ratioing the single-beam reflectance spectrum for the monolayer (R) to the single-beam reflectance spectrum of the cleaned water surface (R_0) and the absorbances ($-\log_{10}(R/R_0)$) calculated. Data analysis, including multiple-point baseline correction, was performed using GRAMS/386 software (Galactic Industries).

Vibrational frequencies, peak widths at half peak maximum, peak heights and integrated peak areas for $\nu_a(\text{CH}_2)$ and $\nu_s(\text{CH}_2)$ were calculated using a center-of-gravity algorithm [12].

3. Results

3.1. Surface pressure—molecular area isotherms

The Π — \hat{A} isotherms from monolayers of PA at 292 and 297 K are shown in Fig. 1. These isotherms define the surface pressure limits of the various monolayer phases and show the phase transitions. More extensive studies by Lundquist [13] and Peterson and colleagues [14–17] have revealed a complex polymorphism for monolayers of fatty acids and Peterson has produced a generic phase diagram in which the phase boundaries change systematically with acyl chain length. Structural studies by, for example, grazing incidence synchrotron X-ray diffraction, have revealed details of the molecular structures of some of these phases [17–23]. In Fig. 1 the various phases have been identified by means of the generic phase diagram and their classifications are

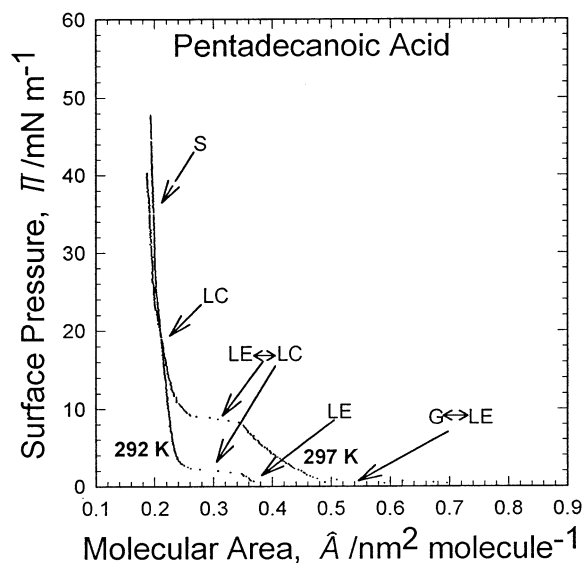


Fig. 1. Representative Π — \hat{A} isotherms for monolayers of PA at the A/W interface at 292 and 297 K. Regions for the various monolayer phases and phase transitions are shown.

shown on the isotherms: LE (or L_1), liquid expanded; LC (L_2), liquid condensed; S (S or LS), 'solid'. The G, gaseous, phase is not seen. Three phase transitions are present: the $G \leftrightarrow LE$ coexistence region which occurs at surface pressures below the sensitivity of the instrument; the $LE \leftrightarrow LC$ coexistence region ($1.6 \pm 0.1 \text{ mN m}^{-1}$ at 292 K and $8.1 \pm 0.1 \text{ mN m}^{-1}$ at 297 K); and the $LC \leftrightarrow S/LS$ second-order transition ($26 \pm 1 \text{ mN m}^{-1}$ at both temperatures).

At surface pressures above 30 mN m^{-1} the PA monolayers exhibited some instability. In such cases the automatic control that maintained constant surface pressure during the recording of a RA FT-IR spectrum was required to decrease the area continually. Such instability has been noted previously by many workers and has recently been studied and discussed by Hifeda and Rayfield [24].

3.2. RA FT-IR spectra in the C–H stretching region

The RA FT-IR spectra of the C–H stretching vibration region ($3000\text{--}2800 \text{ cm}^{-1}$) are shown in Figs. 2 and 3. The spectra were obtained at surface pressures that represent particular phases of the monolayer as defined by the $\Pi\text{--}\hat{A}$ isotherm. For clarity in presentation, some spectra have been shifted on the absorbance scales. The spectra have been plotted as absorbance ($-\log_{10}(R/R_0)$) against wavenumber, where R and R_0 are respectively the single beam reflectance/absorbances of the monolayer-covered surface and the clean water surface. Figs. 2 and 3 demonstrate that a high signal-to-noise ratio can be obtained even at relatively low monolayer surface pressures. However it is important to recognise that the absorbance values are extremely low.

Spectra in the $1900\text{--}1300 \text{ cm}^{-1}$ region were complicated by the presence of water vapour rotation-vibration bands of sufficient intensity to preclude the identification of bands from molecular subgroups within the monolayer (particularly those from the head groups). Background correction and subtraction of reference water vapour spectra did not adequately remove the water vapour bands so these spectra are not presented or discussed.

4. Discussion

4.1. RA FT-IR spectra in the C–H stretching region

Decreases in the observed peak frequencies for the conformation sensitive methylene stretching vibrations have been empirically correlated with an increase in the relative number of *trans* conformers with a concomitant reduction in *gauche* defects within the alkyl chains of the monolayer [25–32]. However quantitative correlations between the magnitude of the frequency shifts and the extent of ordering have yet to be established. A reduction in the number of *gauche* conformers results in a decrease in the cross-sectional area of the alkyl chain and an increase in its overall length [33] so the minimum molecular area occurs when the chain is in the coplanar all-*trans* conformation.

The most obvious difference between RA FT-IR spectra obtained from monolayers on water and those obtained from thin films on reflective metal substrates is the negative absorbance bands observed for the monolayer on water. RA bands may be positive or negative depending on the polarisation of the incident radiation, the proximity of the angle of incidence to the Brewster angle, the direction of the change in dipole moment during the normal mode of vibration [34], and the complex refractive index of the substrate [1,6,35–37]. Negative absorbance bands have been observed by Dluhy and coworkers [1–3,5,10] from phospholipid monolayers at the A/W interface.

In RA FT-IR spectroscopy at the A/W interface three bands are usually resolved in the carbon-hydrogen stretching region. The strongest bands are the antisymmetric and symmetric methylene stretching vibrations ($\nu_a(\text{CH}_2)$ and $\nu_s(\text{CH}_2)$) at $\sim 2920 \text{ cm}^{-1}$ and $\sim 2850 \text{ cm}^{-1}$, respectively. They are clearly seen in Figs. 2 and 3. For an all-*trans* alkyl chain the dipole transition moments of $\nu_a(\text{CH}_2)$ and $\nu_s(\text{CH}_2)$ are perpendicular to the chain axis with the antisymmetric stretching vibration perpendicular to the H–C–H angle bisector and the symmetric stretching vibration parallel to it [7].

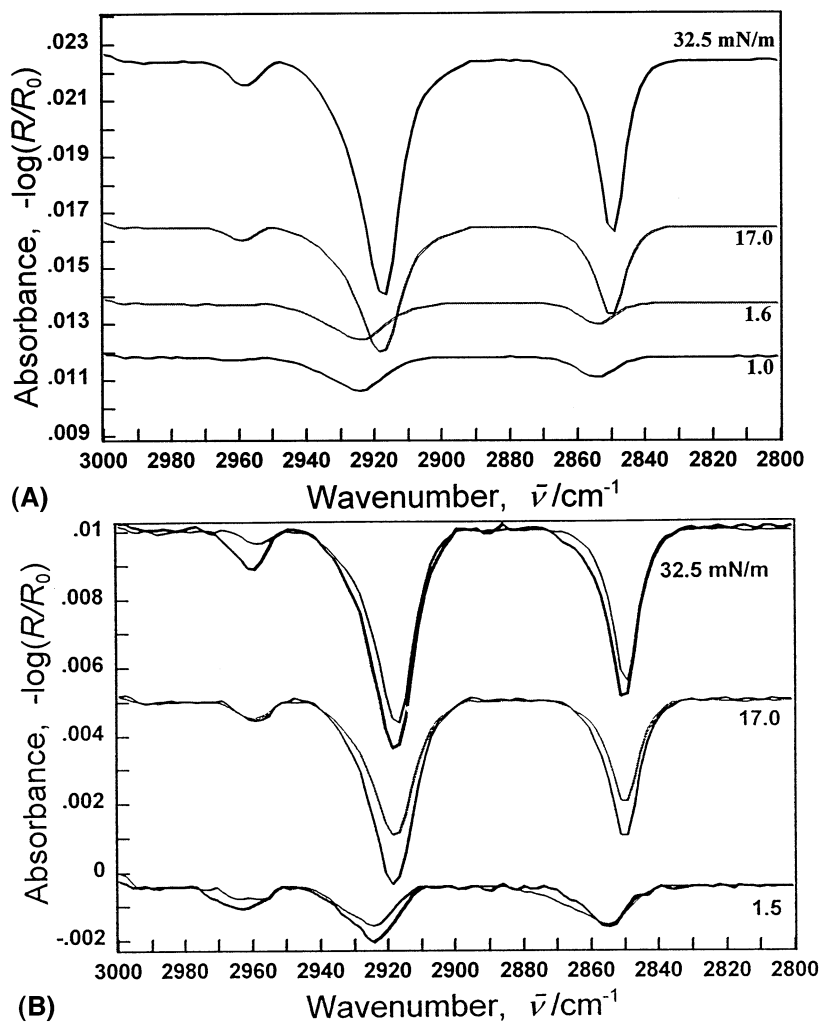


Fig. 2A. RA FT-IR spectra of the C–H stretching vibration region from a monolayer of PA at the A/W interface at 292 K and the surface pressures shown. Unpolarized IR radiation at incidence angle of 30°. B. RA FT-IR spectra of the C–H stretching vibration region from a monolayer of PA at the A/W interface at 292 K and the surface pressures shown. Heavy lines, *p*-polarised; light lines, *s*-polarised IR radiation at incidence angle of 30°.

The methyl stretching vibrations are much less intense than the corresponding methylene stretching vibration bands. In Figs. 2 and 3 the methyl antisymmetric stretching band ($\nu_a(\text{CH}_3)$) is visible at $\sim 2956 \text{ cm}^{-1}$, but the methyl symmetric stretching band ($\nu_s(\text{CH}_3)$) at $\sim 2872 \text{ cm}^{-1}$ lies underneath the other acyl chain vibrational modes and is typically not seen in monolayer spectra at the A/W interface.

It is evident from the spectra in Figs. 2 and 3 that there are decreases in peak frequency and

peak width and increases in peak height and integrated peak area for both of the methylene stretching vibrations as the surface pressure of the monolayer is increased. These changes are shown in Figs. 4–6.

4.1.1. Wavenumber dependence of $\nu_a(\text{CH}_2)$ and $\nu_s(\text{CH}_2)$ on surface pressure

The dependence of the frequencies of the methylene stretching vibrations on surface pressure are shown in Fig. 4. At surface pressures

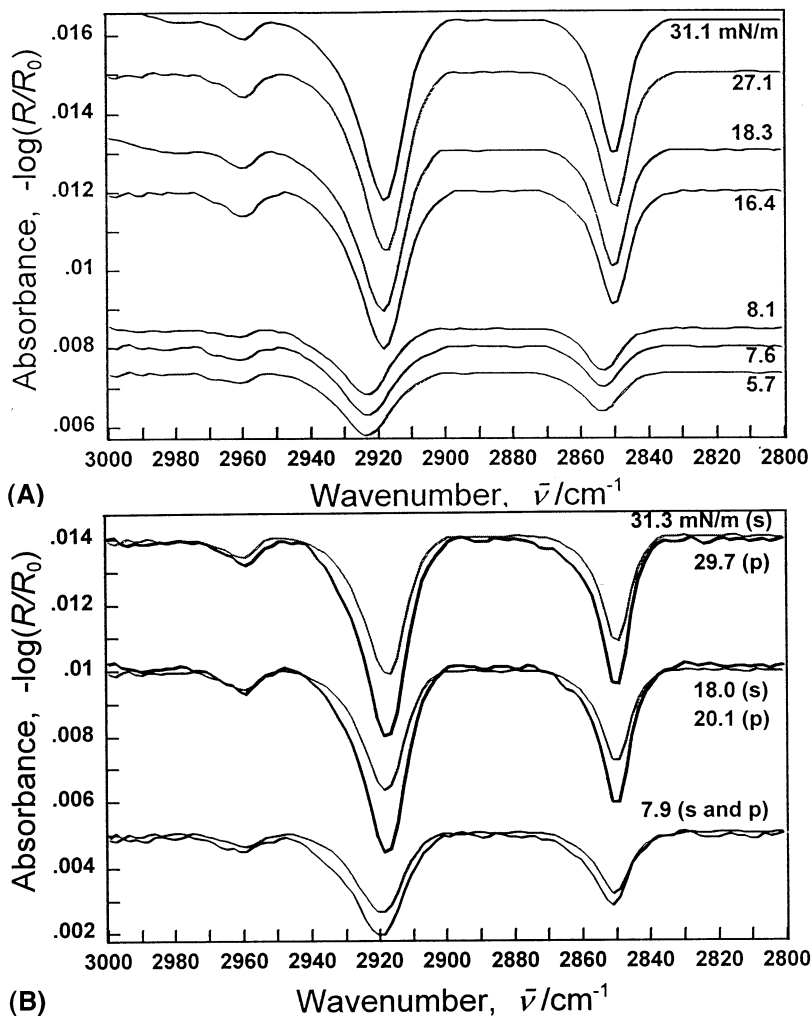


Fig. 3. A. RA FT-IR spectra of the C–H stretching vibration region from a monolayer of PA at the A/W interface at 297 K and the surface pressures shown. Unpolarized IR radiation at incidence angle of 30°. B. RA FT-IR spectra of the C–H stretching vibration region from a monolayer of PA at the A/W interface at 297 K and the surface pressures shown. Heavy lines, *p*-polarised; light lines, *s*-polarised IR radiation at incidence angle of 30°.

below the LE↔LC transition the wavenumber values for polarised and unpolarised radiation at both temperatures were near 2923 and 2854 cm^{-1} for $\nu_a(\text{CH}_2)$ and $\nu_s(\text{CH}_2)$ respectively. These values are in good agreement with the values of $\sim 2926 \text{ cm}^{-1}$ and $\sim 2855 \text{ cm}^{-1}$ that have been observed for polymethylene chains in the liquid phase [3], and thus confirm the liquid-like character of the methylene chains of the PA

monolayer in the LE state and indicate that the chains have a high *gauche* defect concentration and are highly disordered. However the results are in contrast to those obtained by Gericke and Hühnerfuss [8] at 288 and 294 K. Their results showed that for areas corresponding to the LE region there was a large decrease in IR peak frequency (from 2923 to 2919 cm^{-1} for $\nu_a(\text{CH}_2)$) upon approaching the onset of

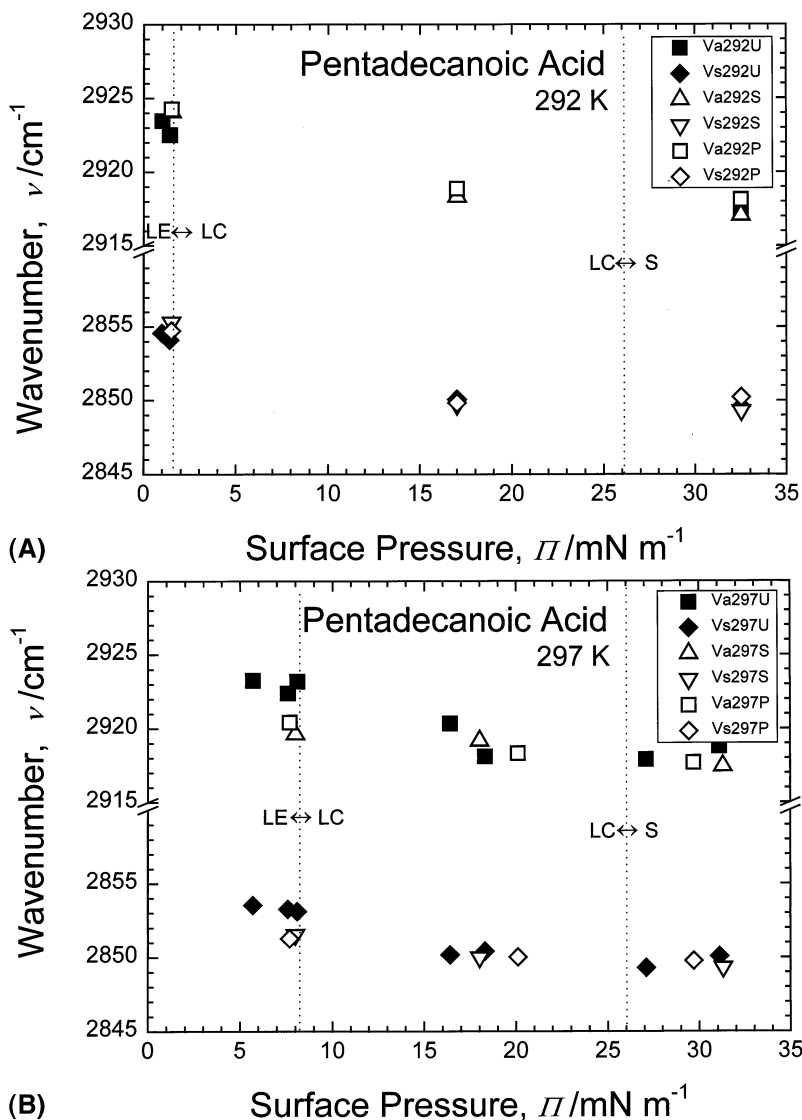


Fig. 4. Wavenumber dependence of $\nu_a(\text{CH}_2)$ and $\nu_s(\text{CH}_2)$ on the surface pressure of a PA monolayer at the A/W interface at the temperatures indicated. Codes in box refer to: $\nu_a(\text{CH}_2)$, Va; $\nu_s(\text{CH}_2)$, Vs; temperature; unpolarised, U; *s*-polarised, S; *p*-polarised, P. Dotted lines indicate the surface pressures of phase transitions.

the LE↔LC coexistence region. This would indicate a strong increase in conformational order during compression through the LE phase if their area determinations are correct.

Only small decreases in peak frequency were observed with unpolarised radiation for $\nu_a(\text{CH}_2)$ and $\nu_s(\text{CH}_2)$ at both temperatures when the monolayer was compressed from the LE region to

the LE↔LC coexistence region (Fig. 4). This similarity indicates that a higher proportion of LE domains than LC domains was sampled by the IR beam in the coexistence region and that the molecular area was near the high area end of this region.

Obvious shifts to lower wavenumbers were observed when the monolayer was compressed from

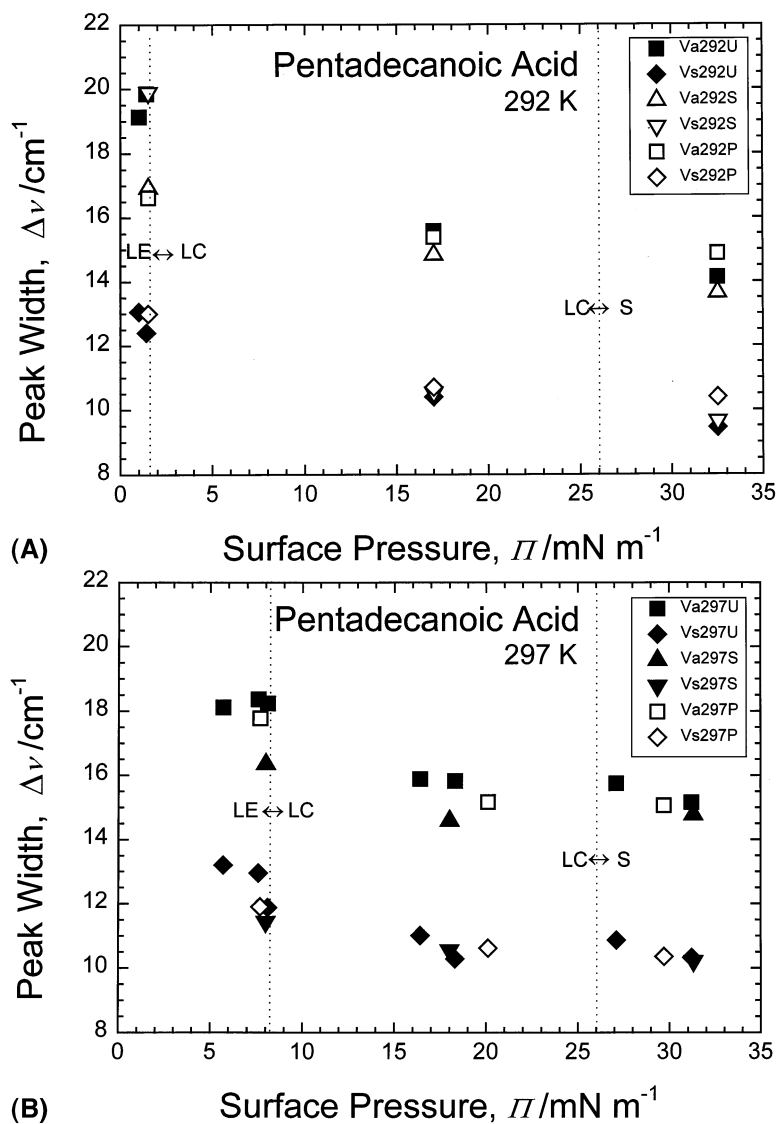


Fig. 5. Dependence of the peak width of $\nu_a(\text{CH}_2)$ and $\nu_s(\text{CH}_2)$ on the surface pressure of a PA monolayer at the A/W interface at the temperatures indicated. Boxed codes and dotted lines as for Fig. 4.

the $\text{LE} \leftrightarrow \text{LC}$ coexistence region to the LC phase, but there were no significant changes in the peak frequency at the transitions from the LC phase to the S phase.

Fewer data were obtained for *s*- and *p*-polarised IR radiation (Fig. 4) but they conform to the same pattern observed with unpolarised radiation. This interpretation allows for the nearly constant surface pressure throughout the $\text{LE} \leftrightarrow \text{LC}$ coexis-

tence region so that measurements at this surface pressure may be sampling near the high area end where the monolayer is dominated by the LE phase or near the low area end where the condensed state is predominant. Thus the data for 292 K were probably obtained near the high area end of the $\text{LE} \leftrightarrow \text{LC}$ coexistence region while the data for 297 K were obtained near the low area end.

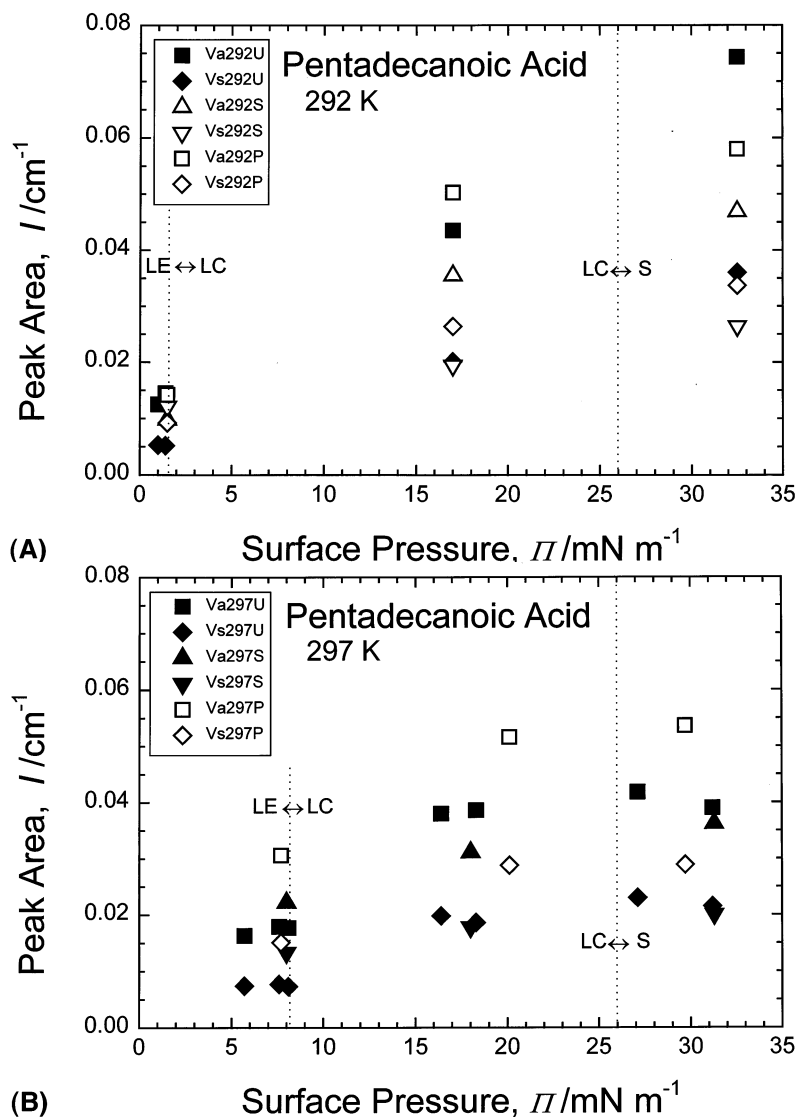


Fig. 6. Dependence of the integrated peak area of $\nu_a(\text{CH}_2)$ and $\nu_s(\text{CH}_2)$ on the surface pressure of a PA monolayer at the A/W interface at the temperatures indicated. Boxed codes and dotted lines as for Fig. 4.

At higher surface pressures, corresponding to the LC and S phases, approximately similar wavenumber values were obtained with unpolarised and both *s*- and *p*-polarised IR radiation at both temperatures (Fig. 4). These values agree with values that have been established [3] as characteristic of highly ordered mostly all-*trans* conformations of the alkyl chains arranged in a crystalline lattice: i.e. wavenumbers of ~ 2917

cm^{-1} and $\sim 2849 \text{ cm}^{-1}$ for $\nu_a(\text{CH}_2)$ and $\nu_s(\text{CH}_2)$, respectively.

The difference between the results obtained in this study and those obtained by Gericke and Hühnerfuss [8] may be due to the different size of the focal point of the IR beam on the water surface, different sizes of the monolayer domains or to the different sampling times (approximately 8 min for one spectrum in this study compared to

approximately 3–4 min for one spectrum in the Gericke–Hühnerfuss study). This explanation, given by Gericke and Hühnerfuss [8], was used to account for the strong scatter in the methylene wavenumber values that was observed by Dluhy et al. [10] in the LE↔LC coexistence region from a monolayer of DPPC compared to their result from a monolayer of PA where there was no scatter in the coexistence region. However it should be noted that Gericke and Hühnerfuss used the miniature Langmuir trough of the modified reflection/absorption attachment of SPECAC (Orpington) and were only able to estimate surface pressures from the area data. Our experience indicates that, because of the very small area of the subphase surface, this procedure is prone to large errors.

Overall, the wavenumber results for $\nu_a(\text{CH}_2)$ and $\nu_s(\text{CH}_2)$ are in agreement with the conclusions of Shen and coworkers [38] who used infrared-visible sum-frequency generation vibrational spectroscopy. They concluded that in the LC phase the long alkyl chains of the PA molecules adopt an all-trans conformation and are oriented normal to the surface, while in the LE phase the chains are deformed (i.e. possess a high concentration of *gauche* conformers) and are orientationally disordered.

4.1.2. Dependence of the peak width of $\nu_a(\text{CH}_2)$ and $\nu_s(\text{CH}_2)$ on surface pressure

The dependence on surface pressure of the peak widths (at half maximum peak height) of $\nu_a(\text{CH}_2)$ and $\nu_s(\text{CH}_2)$ are shown in Fig. 5. The width of the absorbance peak is dependent on the rotational motion and flexibility of the methylene chains [30,31,39–41], with increased widths resulting from an increased mobility and flexibility [42]. Furthermore an increase in the hydrocarbon chain mobility reflects a reduction in the lateral interchain interactions and also indicates the presence of *gauche* rotamers.

The data plotted in Fig. 5 show patterns that are similar to those for peak frequency in Fig. 4 and thus support the interpretation given for that data. At surface pressures below the LE↔LC coexistence region the peak widths are relatively large indicating *gauche* conformers and disorder,

whereas at surface pressures above the LE↔LC transition the peaks are relatively narrow and indicate few *gauche* defects and highly-ordered structures. Within the LE↔LC transition region the data can vary between these two extremes depending on the position within the region where the spectra were recorded.

Possibly there is also a small reduction in peak width at 292 K attributable to the transition (at $26 \pm 1 \text{ mN m}^{-1}$) from the LC phase to the S phase (Fig. 5), although there are no corresponding changes in the peak frequencies (Fig. 4). These results could reflect a small increase in order and packing density during the transition and possibly a decrease in the chain tilt angle. In the S phase the hydrocarbon chains are expected to be oriented perpendicular to the plane of the surface and to possess a structure related to that of a three-dimensional crystal. There are no similar changes in peak width at 297 K.

4.1.3. Dependence of the peak height and integrated peak area of $\nu_a(\text{CH}_2)$ and $\nu_s(\text{CH}_2)$ on surface pressure

The values of the peak height and integrated peak area of the methylene stretching bands provide information on the density of film molecules (number of molecules per unit film area). The dependence on surface pressure of the integrated peak areas of $\nu_a(\text{CH}_2)$ and $\nu_s(\text{CH}_2)$ are shown in Fig. 6. Peak height data follow similar patterns and are not presented.

In all cases there is a general tendency for peak height and integrated peak area to increase as the monolayer is compressed from low to high surface pressure but, as before, it is necessary to consider these data in relation to the surface pressure—area isotherms of Fig. 1. Substantial increases in peak area occur when the monolayers are compressed from the LE↔LC coexistence region to the LC region and reflect the large differences in surface concentration between the high area end of the transition region and the condensed state. The $\Pi-\hat{A}_M$ isotherms (Fig. 1) are very steep in the condensed states (LC and S) and consequently there are only small increases in surface concentration as the surface pressure is raised. Thus there are (with one exception) only slight changes in peak area.

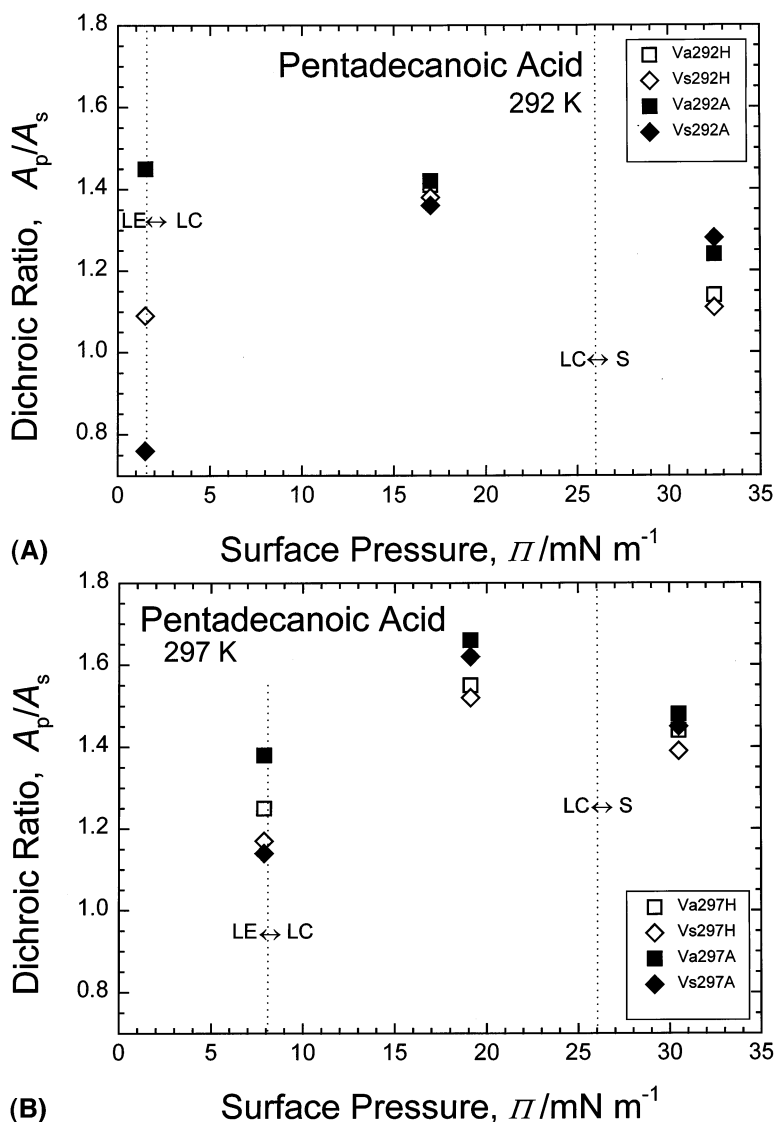


Fig. 7. Dependence of the dichroic ratio on surface pressure for $\nu_a(\text{CH}_2)$ and $\nu_s(\text{CH}_2)$ for a monolayer of PA at the A/W interface at the temperatures indicated. Boxed codes as for Fig. 4 plus: calculated from peak heights, H; calculated from peak areas, A.

Increases in the integrated peak area of $\nu_a(\text{CH}_2)$ and $\nu_s(\text{CH}_2)$ as the monolayer is compressed result not only from an increase in the concentration of film molecules on the surface but may also arise from a change in the direction of the dipole moment for the stretching vibration indicating a decrease in the average tilt angle of the ordered hydrocarbon chains [7,43,44]. Gericke et al. [45,46] have made extensive use of relative peak

intensities and integrated peak areas for $\nu_a(\text{CH}_2)$ to gain qualitative information on changes in the tilt angle.

Further large increases in peak height and integrated peak area were observed for $\nu_a(\text{CH}_2)$ and $\nu_s(\text{CH}_2)$ at 292 K when the molecules underwent the transition from the LC phase to the S phase. This result can be attributed to decreases in the concentration of *gauche* defects and decreases in

tilt angle and is correlated with the previously noted decreases in peak width during this phase transition. However such changes were not observed at 297 K, corresponding again with the peak width results.

Of particular interest in Fig. 6 are the comparisons between *s*- and *p*-polarized radiation. For a particular peak, the areas are similar when the monolayer is in the LE state or the LE↔LC transition but diverge when the condensed states are reached: the peak areas for *p*-polarised radiation exhibiting significantly larger increases than the peak areas for *s*-polarised radiation.

Thus both the antisymmetric and symmetric methylene stretching vibrations exhibit the phenomenon of dichroism. Dichroism which is a key parameter in the determination of molecular orientation information may be defined by a dichroic ratio, D , where $D = A_p/A_s$ (A_p and A_s refer to the absorbance intensities of the vibrational band obtained respectively with *p*-polarised radiation and with *s*-polarised radiation). Dichroic ratios were determined from values of the peak height and integrated peak area and are presented in Fig. 7.

Buontempo and co-workers [47,48] have claimed that an observed insensitivity of the dichroic ratio to a decrease in monolayer surface area implies that there is no change in the collective tilt of the hydrocarbon chains. Fig. 7 shows that the dichroic ratios depend on the surface pressure (or molecular area) and indicate that there is a change in the collective tilt of the hydrocarbon chains as the surface pressure is increased. Values only slightly greater than 1 at 31 mN m⁻¹ imply a small angle of tilt in the S phase, larger values at 16 or 18 mN m⁻¹ suggest larger tilt angles in the LC phase, while the (mostly) low values near the LE↔LC transition pressures could be attributable to more disordered molecular arrangements.

5. Conclusions

The structures of monolayers of pentadecanoic acid have been investigated by RA FT-IR spec-

troscopy over a range of surface pressures at pH = 2 and at 292 and 297 K. Evidence of monolayer structure and structural change is provided mainly by details of the carbon-hydrogen antisymmetric and symmetric stretching vibrations: peak position (wavenumber), peak width, peak height and peak area results all contribute to and support the analysis.

At surface pressures that correspond to the LE phase the acyl chains are found to be disordered and to possess a high concentration of *gauche* defects, whereas at surface pressures that correspond to the LC and S phases the acyl chains are highly ordered and adopt a mostly all-*trans* conformation.

Spectra for the LE↔LC coexistence region depend on the molecular area at which they were obtained. There is little change in surface pressure through this region but substantial change in molecular area. At the high area end of the region, where most spectra were acquired, the spectra were similar to those of the LE region. The few spectra from this coexistence region with characteristics that correspond more closely to those of the LC phase are assumed to have been obtained from monolayers at lower areas. There is thus a decrease in the rotational motion and flexibility of the methylene chains as the molecules undergo the LE→LC phase transition.

These changes correlate well with the expected reduction in rotational motion and flexibility of the acyl chains as the surface pressure increases due to the increases in the packing density of the monolayer molecules shown by the surface pressure—molecular area isotherms.

Acknowledgements

B.F.S. wishes to thank the Department of Chemistry, University of Georgia for its hospitality during these experiments, and the Department of Chemistry, University of Queensland for providing financial assistance. This work was supported by the US Public Health Service through National Institutes of Health grant GM40117 (R.A.D.).

References

- [1] R.A. Dluhy, *J. Phys.Chem.* 90 (1986) 1373–1379.
- [2] M.L. Mitchell, R.A. Dluhy, *J. Am. Chem. Soc.* 110 (1988) 712–718.
- [3] R.A. Dluhy, N.A. Wright, P.R. Griffiths, *Appl. Spectrosc.* 42 (1988) 138–141.
- [4] R.A. Dluhy, M.L. Mitchell, T. Pettenski, J. Beers, *Appl. Spectrosc.* 42 (1988) 1289–1293.
- [5] R.A. Dluhy, D.G. Cornell, *J. Phys.Chem.* 89 (1985) 3195–3197.
- [6] R.A. Dluhy, S.M. Stephens, S. Widayati, A.D. Williams, *Spectrochim. Acta. Part A* 51 (1995) 1413–1447.
- [7] R. Mendelsohn, J.W. Brauner, A. Gericke, *Ann. Rev. Phys. Chem.* 46 (1995) 305–334.
- [8] A. Gericke, H. Hühnerfuss, *J. Phys. Chem.* 97 (1993) 12899–12908.
- [9] A. Gericke, H. Hühnerfuss, *Langmuir* 11 (1995) 225–230.
- [10] R.D. Hunt, M.L. Mitchell, R.A. Dluhy, *J. Mol. Struct.* 214 (1989) 93–109.
- [11] R.A. Dluhy, K.E. Reilly, R.D. Hunt, M.L. Mitchell, A.J. Mautone, R. Mendelsohn, *Biophys. J.* 56 (1989) 1173–1181.
- [12] D.G. Cameron, J.K. Kauppinen, D.J. Moffatt, H.H. Mantsch, *Appl. Spectrosc.* 36 (1982) 245–250.
- [13] M. Lundquist, *Chemica Scripta* 1 (1971) 5–20, 197–209.
- [14] A.M. Bibo, C.M. Knobler, I.R. Peterson, *J. Phys. Chem.* 95 (1991) 5591–5599.
- [15] A.M. Bibo, C.M. Knobler, I.R. Peterson, *Macromol. Chem. Macromol. Symp.* 46 (1991) 55–64.
- [16] A.M. Bibo, I.R. Peterson, *Adv. Mat.* 2 (1990) 309–311.
- [17] R.M. Kenn, C. Bohm, A.M. Bibo, I.R. Peterson, H. Mohwald, J. Ms-Nielsen, K. Kjaer, *J. Phys. Chem.* 95 (1991) 2092–2097.
- [18] B. Lin, M.C. Shih, T.M. Bohanon, G.E. Ice, P. Dutta, *Phys. Rev. Lett.* 65 (1990) 191–194.
- [19] M.C. Shih, T.M. Bohanon, J.M. Mikrut, P. Zschack, P. Dutta, *Phys. Rev. A* 45 (1992) 5734–5737.
- [20] S.W. Barton, A. Goudot, O. Bouloussa, F. Rondelez, B. Lin, F. Novak, A. Acero, S.A. Rice, *J. Chem. Phys.* 96 (1992) 1343–1351.
- [21] M.L. Schlossman, D.K. Schwartz, P.S. Pershan, E.H. Kawamoto, G.J. Kellog, S. Lee, *Phys. Rev. Lett.* 66 (1991) 1599–1602.
- [22] K. Kjaer, J. AlsNielsen, C.A. Helm, P. Tippman-Krayer, H. Mohwald, *J. Phys. Chem.* 93 (1989) 3200–3206.
- [23] K. Kjaer, J. AlsNielsen, C.A. Helm, P. Tippman-Krayer, H. Mohwald, *Thin Solid Films* 159 (1988) 17–28.
- [24] Y.F. Hifeda, G.W. Rayfield, *Langmuir* 8 (1992) 197–200.
- [25] R.A. McPhail, H.L. Strauss, R.G. Snyder, C.A. Elliger, *J. Phys. Chem.* 88 (1984) 334–341.
- [26] R.A. Dluhy, D.G. Cameron, H.H. Mantsch, R. Mendelsohn, *Biochemistry* 22 (1983) 6318–6325.
- [27] R.G. Snyder, H.L. Strauss, C.A. Elliger, *J. Phys. Chem.* 86 (1982) 5145–5150.
- [28] R.G. Snyder, S.L. Hsu, S. Krimm, *Spectrochim. Acta* 34A (1978) 395–406.
- [29] H. Sapper, D.G. Cameron, H.H. Mantsch, *Can. J. Chem.* 59 (1981) 2543–2549.
- [30] H.L. Casal, H.H. Mantsch, *Biochim. Biophys. Acta* 779 (1984) 381–401.
- [31] J. Umemura, D.G. Cameron, H.H. Mantsch, *Biochim. Biophys. Acta* 602 (1980) 32–44.
- [32] H.L. Casal, D.G. Cameron, H.H. Mantsch, *Can. J. Chem.* 61 (1983) 1736–1742.
- [33] G.M. Bell, L.L. Combs, L.J. Dunne, *Chem. Rev.* 81 (1981) 15–48.
- [34] B. Pastrana-Rios, C.R. Flach, J.W. Brauner, A.J. Mautone, R. Mendelsohn, *Biochemistry* 33 (1994) 5121–5127.
- [35] A. Gericke, A.V. Michailov, H. Hühnerfuss, *Vib. Spectrosc.* 4 (1993) 335–348.
- [36] J.D.E. McIntyre, in: R.H. Muller (Ed.), *Advances in Electrochemistry and Electrochemical Engineering*, Wiley, New York, 1973, Vol. 9, Ch. 2.
- [37] L.J. Fina, Y. Tung, *Appl. Spectrosc.* 45 (1991) 986–992.
- [38] P. Guyot-Sionnest, J.H. Hunt, Y.R. Shen, *Phys. Rev. Lett.* 59 (1987) 1597–1600.
- [39] R. Mendelsohn, R.A. Dluhy, T. Taraschi, D.G. Cameron, H.H. Mantsch, *Biochemistry* 20 (1981) 6699–6706.
- [40] T. Kawai, J. Umemura, T. Takenaka, M. Kodama, S. Seki, *J. Colloid Interface Sci.* 103 (1985) 56–61.
- [41] D.G. Cameron, J. Umemura, P.T. Wong, H.H. Mantsch, *Colloids Surf.* 4 (1982) 131–145.
- [42] K.A. Wood, R.G. Snyder, H.L. Strauss, *J. Chem. Phys.* 91 (1989) 5255–5267.
- [43] B. Pastrana-Rios, S. Taneva, K.M.W. Keough, A.J. Mautone, R. Mendelsohn, *Biophys. J.* 69 (1995) 2531–2540.
- [44] C.R. Flach, F.G. Prendergast, R. Mendelsohn, *Biophys. J.* 70 (1996) 539–546.
- [45] A. Gericke, R. Mendelsohn, *Langmuir* 12 (1996) 758–762.
- [46] A. Gericke, H. Hühnerfuss, *Ber. Bunsenges. Phys. Chem.* 99 (1995) 641–650.
- [47] J.T. Buontempo, S.A. Rice, *J. Chem. Phys.* 98 (1993) 5835–5846.
- [48] J.T. Buontempo, S.A. Rice, S. Karaborri, J.I. Siepmann, *Langmuir* 9 (1993) 1604–1607.